![x]

Stabilization of noble metal nanostructures for catalysis and sensing

Journal:	*Nanoscale*
Manuscript ID	NR-FEA-08-2018-006757.R1
Article Type:	Feature Article
Date Submitted by the Author:	08-Oct-2018
Complete List of Authors:	Feng, Ji; University of California, Riverside, Chemistry Gao, Chuanbo; Xi'an Jiaotong University, Frontier Institute of Science and Technology Yin, Yadong; University of California Riverside, Department of Chemistry

![x]

Nanoscale

FEATURE ARTICLE

Stabilization of noble metal nanostructures for catalysis and sensing

Ji Feng,[a] Chuanbo Gao,*[b] and Yadong Yin*[a]

Noble metal nanocrystals have been widely used as active components in catalysis and chemical/bio-sensing. The sizes, structures, and shapes of noble metal nanocrystals are crucial to their electronic, optical, and catalytic properties. However, metal nanocrystals tend to lose their structural and morphological properties when they are subjected to thermal and chemical treatment. Therefore, stabilization of noble metal nanostructures remains a challenge. In this feature article, we present our recent efforts on the stabilization of noble metal nanocrystals, i.e., using inorganic and non-metal solids as supports and physical barriers, protecting the nanocrystal surface by a metal coating, and forming alloys with other metals. At the end of this review, we provide our perspectives on the future development of effective methods for nanocrystal stabilization.

1. Introduction

Investigation of noble metal nanocrystals for catalysis and chemical/bio-sensing has attracted constant attention. The design and synthesis of ideal noble metal nanocrystals are one of the most important research fields in chemistry and chemical engineering.[1-6] In 1989, the first report of gold-nanoparticle catalyzed oxidation of carbon monoxide and hydrogen opened a new door for noble metal nanomaterials in catalysis.[7, 8] After this pioneering work, much research has been done to optimize the nanocrystals for improved catalytic performance. It is widely believed that when the size of the catalyst goes down to the nanometer scale, the interaction between the reactant and the catalyst enhances dramatically. Moreover, noble metal nanocrystals with precise design of structure and shape have been proved to show improved performance in catalytic reactions.[9-13] For example, Mostafa et al. investigated the catalytic properties of Pt nanocrystals with different geometric structures and concluded that the undercoordinated Pt surface atoms (corner and edge atoms) are the most active reaction sites.[14] Plasmonic nanostructures, such as Au, Ag and Cu nanoparticles, have received considerable attention in catalysis due to the excitation of their localized surface plasmon resonances (LSPR). LSPR is generated by the interaction of light and the electrons in the conduction band of the metal nanocrystals. This interaction produces coherent localized plasmon oscillations with a resonant frequency, resulting in sharp optical absorption and scattering as well as strong electromagnetic near-field enhancements that depend on the compositions, sizes, geometries and dielectric environments of the nanocrystals.[15, 16] The hot electrons can vibrationally activate adsorbates at the metal surface and catalyze reactions, such as Suzuki coupling, water splitting, ethylene and propylene epoxidation, NH_3 oxidation, and CO oxidation.[17-20] Besides, plasmonic nanostructures have been widely investigated for chemical/bio-sensing. It has been demonstrated that nanostructures with edges or sharp tips show advantages for surface-enhanced Raman scattering (SERS), due to the strong enhancement of electric field intensity on the surface of nanocrystals.[21, 22] Moreover, the refractive index sensitivity is highly enhanced around such geometries. For example, a study on the refractive index sensitivity at the single-particle level showed that silver nanotriangles had a much higher sensitivity than spheres.[23]

Metal nanocrystals without effective protection tend to lose their structural and morphological properties upon thermal or chemical treatment. Due to the high tendency to minimize their surface energy, metal nanocrystals sinter into large aggregates at high temperatures.[24] This process can cause deactivation of the catalysts due to the loss of catalytic surface area and chemical transformation of catalytic phases to non-catalytic phases. For example, after calcination at 1075 K, Pt nanoparticles of 2-3 nm dispersed on silica beads sintered into 10-20 nm large crystals.[25] The large crystals appeared to be much less active than particles with small size. Moreover, the structure of plasmonic metal nanoparticles, such as Ag, is susceptible to chemical etching, which can lead to a decay in the plasmonic property and catalytic/sensing performance.[26-28]

Until now, many physical and chemical approaches to the stabilization of noble metal nanocrystals have been reported. Physical approaches aim to provide a passivation layer on the surface of noble metal nanocrystals to prevent them from aggregation and sintering. The passivation layer can be composed of organic surfactants or inorganic and nonmetal solids. Various organic surfactants have been used to cap or passivate the surface of the metal nanocrystals, such as polyvinylpyrrolidone (PVP), cetyltrimethylammonium bromide (CTAB), sodium dodecyl sulfate (SDS), polyvinyl alcohol (PVA), and some tri-block copolymers.[29-32] Electrostatic and steric repulsions are the two main forces for the

[a.] Department of Chemistry, University of California, Riverside, California 92521, USA, E-mail: yadong.yin@ucr.edu
[b.] Center for Materials Chemistry, Frontier Institute of Science and Technology and State Key Laboratory of Multiphase Flow in Power Engineering, Xi'an Jiaotong University, Xi'an, Shaanxi 710054, China, E-mail: gaochuanbo@mail.xjtu.edu.cn

stabilization of the metal nanocrystals. Although organic surfactants can help to control the shape of the noble metal nanocrystals and prevent them from aggregation during the long-term reaction, they may also cause deactivation of the catalysts due to the blocking of active sites by the organic ligands, especially when the interaction between the organic surfactant and the metal nanocrystal is strong.[33-36] Surface deactivation caused by organic ligands also happens to sensing. We have shown that Au nanoparticles with clean surfaces exhibit stronger SERS signals than PVP-capped Au nanoparticles.[37] In addition, because of the unstable nature of the surfactants, most of them fail to provide sufficient protection to the metal nanocrystals against aggregation especially in many high-temperature catalytic reactions.

Compared with the cases involving organic ligands, using inorganic and non-metal solids to prevent noble metal nanocrystals from sintering has been proved to be more advantageous. First, inorganic and non-metal solids can act as supports and physical barriers for noble metal nanocrystals to prevent their agglomeration.[38] They can also act as sacrificial templates to fabricate functional yolk-shell nanoparticles.[39] Second, inorganic solids and non-metal materials have better thermal and chemical stability than organic molecules,[40] so that the protection can be maintained at relatively high temperatures. Also, the surface of noble metal nanocrystals can be very clean without organic molecules, preventing decay of performance caused by the capping ligands. Moreover, some inorganic compounds and non-metal materials can participate in catalytic reactions to enhance the performance of the catalysts. For example, graphene has been used as a substrate for anchoring metal nanocrystals for electrocatalysis due to its large specific area, excellent mechanical properties and conductivity. The lattice defects and surface functional groups in chemically converted graphene provides a strong binding for the immobilization of metal nanoparticles.[41] Moreover, the catalytic activity of the graphene-supported catalysts can be enhanced because of the increased charge transfer from the catalysts to graphene substrate.[42]

Inorganic and non-metal solids can protect the noble metal nanocrystals in many ways by acting as supports to noble metal nanocrystals, physical barriers, and sacrificial templates for the fabrication of yolk-shell materials. In the first case, noble metal nanocrystals are dispersed or reduced from their precursors on the surface of the non-metals, including silica, minerals, Fe_3O_4, and carbon.[43-46] It is worth noting that the chemical nature of some oxides can contribute to the functionality of the nanostructures. For example, the magnetic property of Fe_3O_4 can make the nanocrystals recyclable under a magnetic field.[47] Besides supporting metal nanocrystals, non-metals contribute to the stability of noble metal nanocrystals by forming physical barriers.[48] In this case, non-metals are coated on the surface of the metal nanocrystals to form core-shell nanostructures.[20] Metal nanocrystals could benefit from the inactive and porous non-metal layer to survive under harsh reaction conditions. The non-metal nanoshells can also serve as nanoreactors for the synthesis of metal nanocrystals with precisely designed shape and components. They can also act as sacrificial templates to direct the synthesis of metal-oxides core-shell nanostructures with integrated catalytic performances from both metals and the oxides. Besides the stabilization of metal nanocrystals by using non-metals, coating noble metal nanocrystals with metals of higher stabilities can
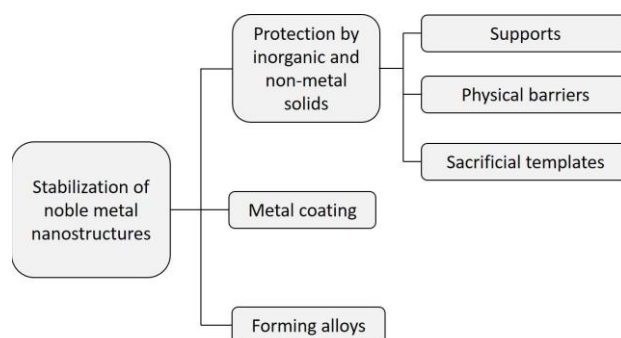

Fig. 1. An overview of methods for the stabilization of noble metal nanostructures.

not only protect them from the corrosive environment but also retain the plasmonic property of their original structures. The excellent optical properties of plasmonic metal nanocrystals, Ag, for example, can be maintained by depositing a layer of Au on its surface to prevent direct contact of Ag nanocrystals with any external etchants.[49] The Ag@Au core-shell nanostructures can show superior activity in SERS detection, and significantly enhanced chemical stability in harsh conditions such as strongly oxidative environments in many practical applications.[50] In addition, the stable Au surface can be further functionalized for bio-sensing.[51, 52]

Moreover, the stabilization of metal nanocrystals by forming an alloy is another effective way to retain the plasmonic properties of metal nanocrystals while enhancing their chemical stability. Conventional Ag/Au alloy nanoparticles can be formed by co-reduction of Au and Ag precursors and galvanic replacement.[53, 54] More recently, our group contributed a method for the fabrication of fully alloyed Ag/Au nanoparticles with high stability based on interfacial atomic diffusion of Ag and Au in a Au@Ag core-shell nanoparticle.[55] The Ag/Au alloy nanoparticles show extremely narrow LSPR bandwidths due to the homogeneous distribution of Ag and Au, minimal crystallographic defects, and the absence of structural and compositional interfaces. As expected, the alloy nanocrystals can also survive harsh conditions, so that the application of the nanocrystals could be greatly broadened, for example, in the monitoring of pollution in many natural and industrial settings.

In this feature article, we aim to summarize a number of strategies toward stabilizing noble metal nanocrystals that were developed in our group. As illustrated in Figure 1, three main categories, including the use of inorganic and non-metal solids, metal coating, and forming alloys will be discussed for the stabilization of noble metal nanocrystals. In the first part, we introduce the role of inorganic compounds and non-metal species as supports, physical barriers and sacrificial templates for the fabrication of yolk-shell nanostructures. In this part, we also discuss the control of the porosity of inorganic shells using a surface-protected etching process. Then we introduce strategies incorporating metals, either as a coating or alloying species, to enhance the stability of the nanocrystals. This feature article is not intended to be a comprehensive summary of the entire field, and we only try to introduce our own efforts in the past few years in addressing the stability issues. There are undoubtedly many other interesting and useful approaches in literature, but we have to leave them out in this feature article.

2. Stabilization of noble metal nanocrystals by inorganic and non-metal solids

2.1. Inorganic and non-metal solids as supports

Remarkable thermal stability of metal nanocrystals could be achieved when deposited onto inorganic and non-metal supports. Inorganic oxides with large surface areas, such as SiO_2, Al_2O_3, and TiO_2, are the most widely used support materials in catalysis.[56]

Generally speaking, metal nanocrystals could be loaded on inorganic/non-metal supports by two routes. The first route includes synthesis of the noble metal nanocrystals and dispersing them on the non-metal supports. Moreover, the second route integrates the reduction and deposition of the noble metal nanocrystals in one step. The metal precursors can be reduced in a solution containing the inorganic/non-metal supports. To ensure efficient loading of the metal nanocrystals, one usually needs to modify the non-metal supports. For example, when loading Au nanoparticles on silica substrates, the surface of silica is usually modified with aminopropyltrimethoxysilane, because the strong interaction between gold and amino group helps to stabilize the Au nanocrystals.[57]

However, when dispersing ultrafine nanocrystals on substrates, the agglomeration of nanocrystals could not be avoided entirely. To overcome this issue, we developed a method to anchor ultrafine Au nanoparticles on thin carbon sheets for catalytic reduction of hydrophilic 4-nitrophenol and hydrophobic nitrobenzene.[58] The carbon supported Au nanoparticles was realized by firstly sandwiching a dense monolayer of ultrafine Au nanoparticles between a silica core and a resin shell, then carbonizing the shell at a high temperature, and finally selective removing the silica core. The shrinkage of the shells during carbonization facilitates partial embedment of the AuNPs on the carbon shell surface and provides superior stability against particle sintering during high-temperature/mechanical post-treatments and catalytic reactions.

2.2. Inorganic and non-metal solids as physical barriers

For preventing noble metal nanocrystals from aggregation, a thin inorganic and non-metal layer can be deposited on the surface of the noble metal nanocrystal to form a physical barrier. Silica is the most commonly used non-metal material for the formation of the physical barrier due to its many advantages. For example, silica is chemically inert, so that it doesn't participate in most of the catalytic reactions over the metal nanocrystals. Moreover, the silica shell is microporous, which makes the nanocrystals accessible to reactants in catalytic reactions. Also, silica can be conveniently functionalized, leading to expanded applications of the core-shell nanoparticles in drug delivery, fluorescence sensing, and imaging.[59, 60]

Typically, silica coating of metal nanocrystals can be achieved using either the modified Stöber method or sol-gel reactions in reverse micelle systems. The modified Stöber method can create a smooth silica layer by adding tetraethoxysilane (TEOS) to a mixture containing metal nanocrystals, ethanol, H_2O, and ammonia. Some nanoparticles, such as titania, zirconia, and other metal oxides can be directly coated by silica due to the strong affinity of the surface with silicate species under reaction conditions. In contrast, it is difficult to directly coat metal nanocrystals with silica because of the lack of affinity. For example, gold and silver can only be coated with silica with the help of sodium silicate, surfactants, or coordinating
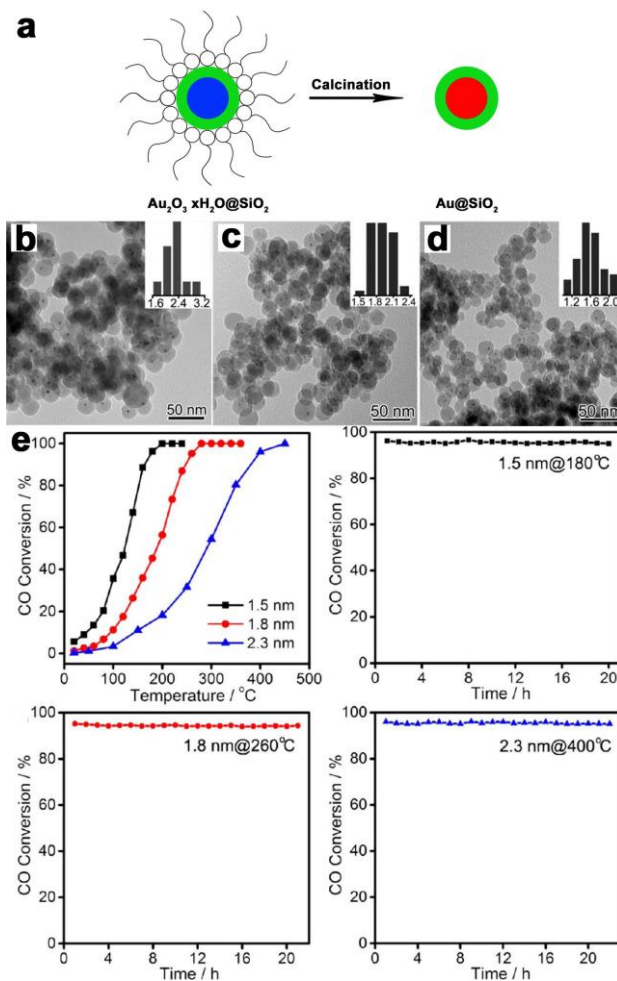

Fig. 2. (a) Schematic illustration of coating silica on ultra-small Au nanoparticles. (b-d) TEM images of Au@SiO$_2$ nanoparticles with average core sizes of 2.3, 1.8, and 1.5 nm, respectively, obtained after annealing at 200 ºC. Inset: size distributions of the cores in nanometers. (e) Catalytic CO oxidation of the Au@SiO$_2$ core-shell nanospheres and plots of CO conversion versus reaction time. Reprinted and modified from Ref. [69] with permission. Copyright 2014 American Chemical Society.

silanes.[61] It is worth noting that the silica coating in reverse micelle systems always results in well disperse core-shell nanoparticles. The system is composed of metal nanocrystals, polar solvents, non-polar solvents, ammonia, amphiphilic surfactants, and silica precursors. In a typical synthesis, microemulsion droplets of the polar solvents can be stabilized by amphiphilic surfactants in the non-polar solvents. The hydrolysis and condensation process of TEOS can occur inside the microemulsion droplets. Metal nanocrystals, such as Au, Ag, Pt, Pd, Rh, and Ni have been successfully coated in reverse micelle systems.[62-67]

When the nanocrystals are ultra-small (< 3 nm), conventional methods fail to produce a metal-silica core-shell structure due to the insufficient interaction between noble metal nanoparticles and silicate oligomers.[68] We have therefore reported a method to coat ultra-small Au@SiO$_2$ core-shell nanostructures.[69] To enhance the chemical affinity of the core to the shell, we employed ultra-small
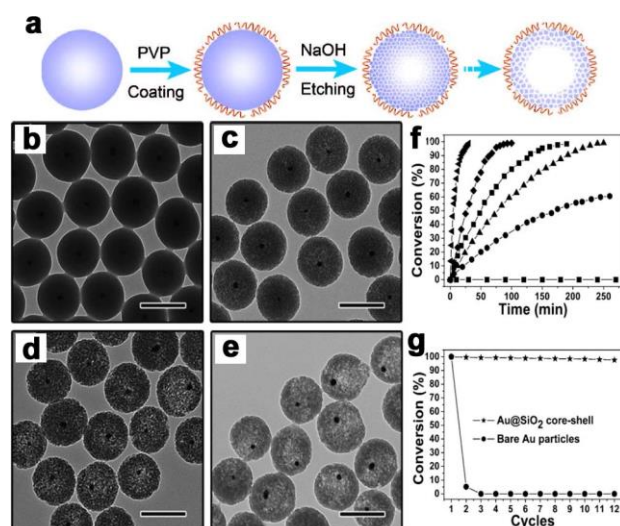
Fig. 3. (a) Schematic illustration of the concept of surface-protected etching for transforming solid structures into hollow structures with permeable shells. TEM images showing the structure evolution of Au@SiO$_2$ core-shell particles: (b) original sample; and samples after etching with NaOH for (c) 2 h; (d) 2 h 45 min; and (e) 3 h. All scale bars are 200. (f) Conversion of 4-NP using Au@SiO$_2$ catalysts that have been etched in NaOH for the following times: ■ 0 min; ● 1 h 30 min; ▲ 2h; ▼ 2 h 30 min; ◆ 2 h 45 min; and ◄ 3 h. f) Conversion of 4-NP in 12 successive cycles of reduction with Au@SiO$_2$ yolk-shell structure; and bare Au nanoparticles. Reprinted and modified from Ref. [71] with permission. Copyright 2008 American Chemical Society.

gold hydroxide nanoparticles as precursors to Au nanoparticles. As shown in Figure 2a, by using reverse micelles, the hydrolysis and condensation of silica oligomers could be confined in nanoscale spaces, leading to the reduced size of the silicate oligomers. The surface hydroxyls of the gold hydroxide nanoparticles enabled interactions with silica, which was the key to the formation of a core-shell nanostructure. Then, by annealing at 200 ºC, the Au$_2$O$_3$·xH$_2$O cores were reduced to Au. As shown in Figure 2b-d, Au@SiO$_2$ nanoparticles with core sizes of 2.3, 1.8, and 1.5 nm, and shell thicknesses of 11, 10, and 8.6 nm were synthesized by adjusting the concentration of HAuCl$_4$, the amount of silica precursor and the water to oil ratio. It is worth mentioning that aminosilanes could be used to modify the interface between Au and SiO$_2$, resulting in enhanced stability of the particles under high-temperature treatment (up to 500 ºC). The silica shell was microporous, making the Au core accessible in catalytic reactions.

The resulting Au@SiO$_2$ core-shell nanoparticles were effective and stable catalysts for high-temperature CO oxidation due to the core-shell structure and the stabilization of Au/SiO$_2$ interface by amino groups. At room temperature, all the catalysts showed the negligible conversion of CO. However, as the temperature rose, the conversion of CO rapidly increased and eventually reached ~100 %. The lowest temperature corresponding to the ~100 % conversion of CO was named ~100 % conversion temperature. As shown in Figure 2e, with the decrease of Au particle size from 2.3 to 1.5 nm, the catalytic activity increased, and the ~100 % CO conversion temperature decreases from 400 to 180 ºC. The turnover frequency of the

Au@SiO$_2$ catalysts with core sizes of 2.3, 1.8, and 1.5 nm were 6.64, 46.3, and 96.2 h^{-1}, respectively. All of the particles showed well-maintained catalytic performance after being treated at their ~100 % conversion temperatures for 20 h, indicating high stability of these Au@SiO$_2$ core-shell nanoparticles.

The porosity of the silica shells should be adjusted to some degree to allow the reactants to pass through while maintaining a physical barrier against coalescence of the nanocrystals. The synthesis of silica shells with well-controlled porosity has been achieved by using the soft-templating method. In such a design, some structure-directing surfactants are used to create the pore structures. For example, mesoporous silica encaged Pt nanocrystals have been synthesized by using tetradecyltrimethylammonium bromide as a surfactant.[70] The porous shells significantly enhanced the stability of Pt nanocrystals at temperatures up to 750 ºC in air. Moreover, the mesoporous silica encaged Pt nanocrystals were catalytically as active as bare Pt nanocrystals for ethylene hydrogenation and CO oxidation because the mesopores provided access for the reactants to interact with the Pt core.

Controlled etching of the inorganic/non-metal shells could produce shells with adjustable porosity. We have reported a surface-protected etching method as an effective way to control the porosity of the shells.[71] A schematic illustration of the process is shown in Figure 3a. A typical surface-protected etching process involves polymer molecules, such as polyvinylpyrrolidone (PVP), as the surface protecting agents. PVP molecules bond to silica surface through hydrogen bonding between its carbonyl groups and the hydroxyl groups on the silica surface. It protects the outer shell surface against etching in an aqueous solution of NaOH. The polymer protection allows the core-shell nanoparticles to maintain their original morphology, while the interior silica being selectively etched, resulting in porous shells. The porosity of the shell could be easily tuned by adjusting the etching time of the nanoparticles in NaOH. As the etching time prolonged, the Au@SiO$_2$ nanoparticles became increasingly porous. And finally, a yolk-shell nanostructure could be obtained (Figure 3b-d).[71] The kinetics of the catalytic reactions could be controlled by precisely adjusting the porosity of the silica shell through the surface-protected etching process. As shown in Figure 3f, the reduction of 4-nitrophenol (4-NP) to 4-aminophenol (4-AP) catalyzed by the Au@SiO$_2$ catalyst showed increasing catalytic activity upon more extensive etching of the silica shells. The Au@SiO$_2$ nanocrystals also showed better stability than bare gold nanoparticles. Under the protection of the silica shell, 12 cycles of reaction with ~100 % conversion rate were obtained (Figure 3g). The optical absorption and morphology remained almost unchanged after many cycles of the reaction, indicating the stabilization of Au nanoparticles by the silica shell.

In addition, silica shells can act as nanoreactors for the reaction of the encapsulated materials, which would provide more opportunities in regulating the composition and shape of the core materials.[72] Xiao et al. have demonstrated the formation of Au nanorods from Au spherical seeds by a conventional seeded growth method inside hollow mesoporous shells.[73] The silica shell acts as a physical barrier to ensure the separation of Au seeds during the seeded growth reaction. The metal nanocrystals could be further coated with Pt and Pd. Moreover, the Au nanorods@Pt@SiO$_2$ nanostructures showed high conversion rate and stable cycling

performance toward the oxidation of o-phenylene-diamine (OPDA) by hydrogen peroxide to form 2,3-diaminophenazine (DAP). Another example is the preparation of platinum/iron oxide nanoconjugates confined in silica nanoshells for preferential CO oxidation in H_2 (PROX), which is critically important in proton-exchange membrane fuel cells by allowing selective removal of CO from the feed gas.[74] The synthesis started with the preparation of ultrasmall $(NH_4)_2PtCl_6$ and $Fe(OH)_3$ nanoparticles by co-precipitation of their respective salts in reverse micelles, and the ultrasmall precursor nanoparticles were coated with silica. The precursor nanoparticles were then converted into target Pt/FeO_x nanoconjugates by an alloying-dealloying process, which included an annealing process in CO to reduce and sinter the nanoparticles into alloys, and a dealloying process by annealing the alloys in air to oxidize the less-stable Fe species and form the target Pt/FeO_x nanoconjugates. Herein, the silica shells were employed as nanoreactors to allow the alloy-dealloy process of the nanoparticles without forming aggregates. With the help of the silica shells, the Pt-Fe alloy nanoparticles with the size of 1.6 nm were formed after annealing the $(NH_4)_2PtCl_6$ and $Fe(OH)_3$ nanoparticles in CO atmospheres. After annealing in air, the alloy nanoparticles were readily converted to Pt/FeO_x nanoconjugates with the size of 1.8 nm. The $Pt/FeO_x@SiO_2$ nanospheres showed higher stability than Pt/FeO_x nanoconjugates stabilized on a silica surface. Upon heating at an elevated temperature, the size of the Pt/FeO_x nanoconjugates in silica shells was well retained, while Pt/FeO_x on the silica surface agglomerated to much bigger sizes caused by the Ostwald ripening. The $Pt/FeO_x@SiO_2$ nanospheres showed remarkable catalytic activity and high durability in the PROX reaction. Nearly complete conversion of CO into CO_2 had been achieved at a low temperature of 30 ºC, due to the effect of Pt/FeO_x interface in reducing the activation energy of the oxidation reaction. Moreover, the catalytic activity of the $Pt/FeO_x@SiO_2$ nanospheres became much higher than that of the silica supported Pt/FeO_x nanoparticles at high reaction temperatures (>110 ºC) or after a long reaction time (84 h), thanked to the improved stability of the Pt/FeO_x nanoconjugates against sintering in silica shells compared with those on the surfaces.

2.3. Inorganic and non-metal solids as both supports and physical barriers

Inorganic and non-metal solids can act as both the supports to noble metal nanocrystals and the physical barriers to prevent them from aggregation. This design usually includes three steps: the synthesis of inorganic/non-metal substrates, anchoring the noble metal nanoparticles on the substrates and coating them with a layer of non-metal solids for protection. It may also involve tuning the porosity of the protection layer by chemical etching. We reported silica-supported Pt nanoparticles embedded in mesoporous silica for increased catalyst stability.[25] The catalysts were first prepared by depositing Pt nanoparticles with sizes of 3 nm on 120 nm silica beads. The silica-supported Pt nanoparticles were then covered with a layer of mesoporous silica with a thickness of 20 nm. The outer layer of silica was etched to re-expose the metal surface to the reaction mixtures, while still held Pt nanoparticles trapped in the mesopores. The thermal stability of Pt nanoparticles sandwiched between silica was much better than that of simply dispersing Pt nanoparticles on silica nanospheres. Pt nanoparticles sandwiched between silica could
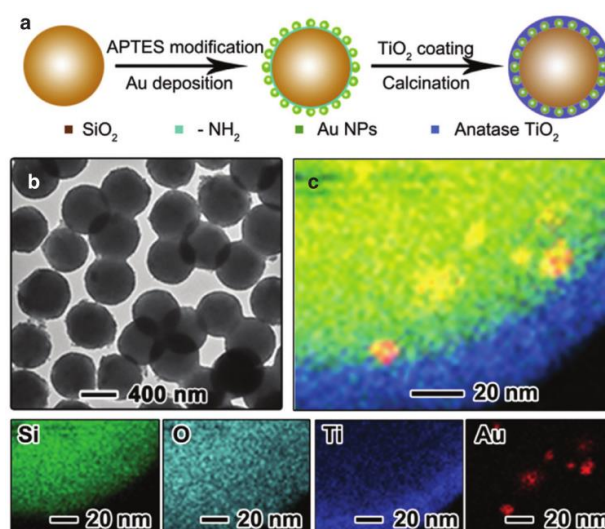

Fig. 4. (a) Schematic illustration of the fabrication process of sandwich-structured $SiO_2@Au@TiO_2$ photocatalysts; (b) a typical TEM image of the composite photocatalyst; (c) elemental mapping of a single particle, with the distribution of individual elements shown in the bottom row. Reprinted and modified from Ref. [75] with permission. Copyright 2011 Wiley-VCH.

resist sintering during calcination at 1075 K, whereas the unprotected Pt nanoparticles were seen to sinter by 875 K.

Another example is the fabrication of Au nanoparticles sandwiched between the silica nanosphere and a layer of mesoporous TiO_2 (Figure 4a).[75] The synthesis required surface modification of silica nanospheres with 3-aminopropyltriethoxysilane, which acted as a ligand for the immobilization of Au nanoparticles on the surface of the SiO_2 nanospheres. The silica-supported Au nanostructures were then coated with TiO_2, followed by calcination in air to crystallize the TiO_2 layer. As shown in Figure 4b, Au nanoparticles with sizes of 5 nm are sandwiched between silica nanospheres with sizes of 400 nm and a layer of TiO_2 of ~20 nm in thickness. It is worth noting that TiO_2 acts not only as a protection layer but also as a photocatalyst, which contributes to the photocatalytic activity. Compared with simply dispersing Au nanoparticles on TiO_2, these sandwich structures had several advantages. First, Au nanoparticles were embedded inside the TiO_2 matrix, which prevented them from agglomerations upon crystallization at high temperatures. As shown in Figure 4c, the sizes of the Au nanoparticles are well maintained after the calcination, indicating high stability of the Au nanoparticles. Second, the encapsulation enabled intimate contact between the Au nanoparticles and the TiO_2 shells and therefore allowed more efficient electron transfer than the previous anchored cases. Moreover, the decomposition of 3-aminopropyltriethoxysilane under high-temperature treatment provided N and C doping to the nanocrystals, contributing to the visible light absorption. In addition, the Au nanoparticles embedded in TiO_2 helped with charge separation of the photogenerated electrons and holes during the photoexcitation of TiO_2. Thus, the nanocomposite showed excellent photocatalytic activity under direct sunlight irradiation. Complete decomposition of RhB could be achieved with the sandwich nanoparticles within 40 min, while only ~38 % and ~27 %

decomposition could be achieved using the commercial P25 photocatalyst and commercial anatase powders.

2.4. Inorganic and non-metal solids as sacrificial templates toward yolk-shell structures

Design of yolk-shell nanostructures with noble metal nanocrystals as yolks has attracted a surge of attention because the shells can act as physical barriers to prevent the cores from sintering. In addition, by building the shells with metal oxides, the yolk-shell nanostructures become new types of catalysts. Generally speaking, the synthesis of yolk-shell nanostructures requires a coating of metal nanocrystals with inorganic/non-metal species, which act as templates for deposition of the shell materials. The inorganic/non-metal layer is sacrificed by chemical etching or calcination under high temperatures. We reported the synthesis of Au@TiO$_2$ yolk-shell nanostructures for the oxidation of carbon monoxide by using silica nanospheres as the sacrificial layers.[76] In this case, Au nanoparticles with a size of 10 nm were prepared first, followed by depositing a thick layer of silica. After that, TiO$_2$ was deposited on the Au@SiO$_2$ nanostructures through a sol-gel method. The Au@SiO$_2$@TiO$_2$ nanostructures were calcined to crystalize TiO$_2$, followed by removal of SiO$_2$ in a NaOH solution. The size of the Au@TiO$_2$ yolk-shell nanospheres was 200 nm, and the thickness of TiO$_2$ was 20 nm. Thanks to the mesoporous nature of TiO$_2$, the Au@TiO$_2$ yolk-shell nanospheres allowed CO molecules to penetrate the TiO$_2$ shells and adsorb on the surface of the Au nanoparticles. The reaction rate of the oxidation of carbon monoxide over Au@TiO$_2$ yolk-shell nanostructures was comparable to that over conventional Au nanoparticles on P25.

3. Stabilization of noble metal nanocrystals by metal coating

Although surface coating with an inorganic/non-metal layer is an effective way to increase the stability of noble metal nanocrystals, it may still fail to meet the requirements of some other applications. For example, silver nanoparticles show superior plasmonic properties to other metal nanoparticles, indicating better performance in sensing, imaging, and catalysis.[77-79] However, the structure of the silver nanoparticles is unstable under many reaction conditions, such as those involving acids, halides, UV irradiation, and heat.[80-82] The stability of silver nanoparticles could be enhanced against etching by coating with silica, which however may become a barrier that prevents the target molecules from accessing the particle surface. Therefore, the sensitivity of the LSPR of silver nanoparticles to the changes in the local environment may be reduced.[83, 84]

The ideal case to stabilize silver nanoparticles is not only to protect them from the corrosive environment but also to maintain the plasmonic and surface property of the original structures. One attempt is to coat silver nanoparticles with gold, which is chemically more inert than silver but closely matches the crystal structure of silver. The key to deposit Au on Ag nanoparticles is to minimize the galvanic replacement reaction. Because the reduction potential of Ag (Ag$^+$/Ag = 0.80 V vs. SHE) is lower than that of Au (AuCl$_4^-$/Au = 0.99 V vs. SHE), Ag is likely to be replaced by Au, forming hollow Au nanostructures.[85] Qin et al. reported a galvanic replacement-free
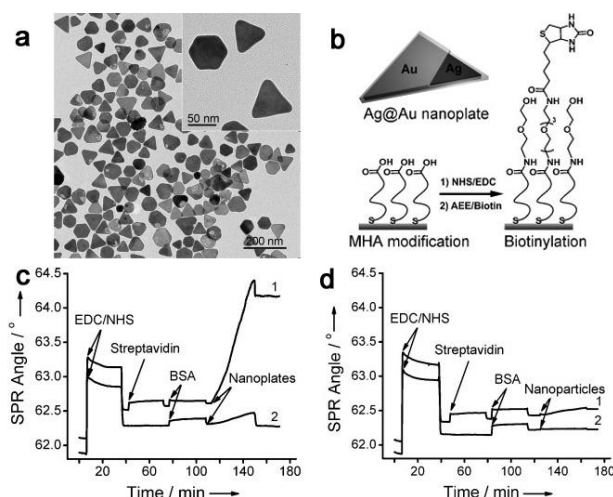

Fig. 5. (a) TEM image of the Ag@Au core/shell nanoplates. (b) Modification of the Ag@Au nanoplates with biotin. (c) 1) Enhancement of SPR angle with the Ag@Au nanoplates as enhancers for detection of streptavidin, and 2) control experiment. (d) 1) Enhancement of SPR angle with conventional Au nanoparticles (16 nm) as enhancers for detection of streptavidin, and 2) control experiment. Reprinted and modified from Ref. [88] with permission. Copyright 2012 Wiley-VCH.

method for the deposition of Au on Ag nanocubes by adjusting the reducing power of the reductants, ascorbic acid.[86] It was shown that the reducing power of ascorbic acid could be enhanced by increasing the pH of the reaction, leading to successfully deposition of Au on Ag without the occurrence of apparent galvanic replacement. Further investigation revealed that when the initial pH was controlled in the range of 10.3-11.9, the reduction of Au(III) was dominated by ascorbic acid, whereas when the initial pH was in the range of 3.2-4.8, the reduction of Au(III) to Au proceeded by both the galvanic replacement with Ag nanocubes and chemical reduction by ascorbic acid.[87]

To minimize the galvanic replacement, our group used I$^-$ to lower the reduction potential of the Au precursor by forming stable complexes.[88] In this approach, PVP was used to bind to the surface of Ag nanoplates via the strong coordination between the N and O atoms and the metal surface. The PVP ligands on Ag surface not only further enhanced the stability of the Ag nanoplates but also prevented these nanoplates from aggregation. A very thin layer of Au (~5 Å) could be deposited on Ag surface by mixing a growth solution, which contained HAuCl$_4$, KI, and PVP, with a mixture composed of PVP, diethylamine, ascorbic acid, and Ag nanoplates. Figure 5a shows the morphology of the Ag@Au core-shell nanoparticles. The plasmonic property was well retained with this thin layer of Au. As the Au layer was homogeneously covering the surface of Ag with good lattice match, the stability of the particles was greatly enhanced against chemical etching in a phosphate buffer solution, a NaCl solution, a phosphate-buffered saline solution, and even an H$_2$O$_2$ solution, compared with bare or 16-mercaptohexadecanoic acid (MHA)-capped Ag nanoparticles. When dispersed in an H$_2$O$_2$ solution (2.1 %), the plasmonic absorption peak of the Au-coated Ag nanoplates remained almost unchanged for 4 days, whereas the
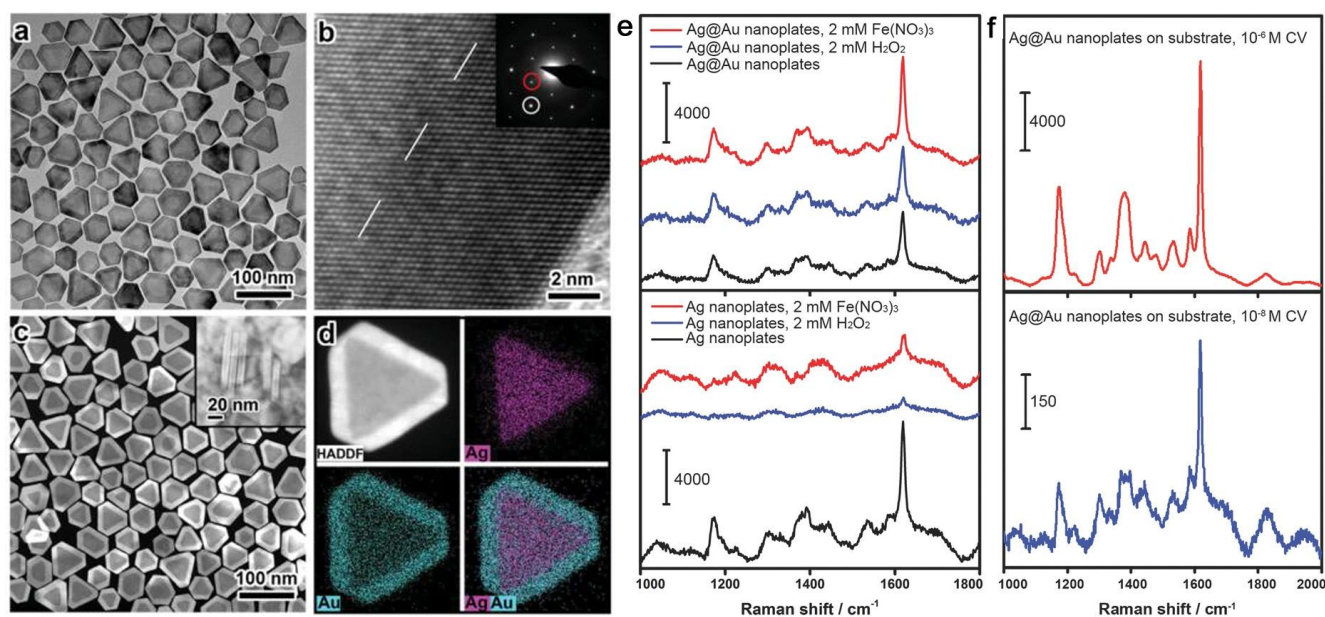
Fig. 6. Synthesis of the truncated triangular Ag@Au core-shell nanoplates. a) TEM image of the nanoplates. b) HRTEM image. The dashed line indicates approximate Ag/Au boundary judged from the image contrast. Inset: Electron diffraction pattern. White and red circles indicate the {220} and formally forbidden 1/3{422} reflections, respectively. c) HAADF-STEM image of the nanoplates. d) EDS elemental mapping of an individual Ag@Au nanoplate. e) SERS spectra recorded from aqueous solutions of crystal violet (CV, 10^{-5} M) enhanced by the Ag@Au and Ag nanoplates in the presence of impurity reagents including Fe^{3+} and H_2O_2. f) SERS spectra of CV with concentrations as low as 10^{-6} M and 10^{-8} M recorded from a silicon substrate deposited with the Ag@Au nanoplates. Reprinted and modified from Ref. [50] with permission. Copyright 2015 Wiley-VCH.

plasmonic absorption peak of bare Ag nanoplates disappeared after 3 minutes.

The as-prepared Ag@Au nanoplates showed excellent performance when used as enhancers for SPR-based bio-sensing. In a typical sensing system, the biotinylated Ag@Au nanoplates were introduced to an 11-mercaptoundecanoic acid and biotin-modified Au film to enhance the SPR response. The scheme for surface modification of Ag@Au nanoplates is shown in Figure 5b. The SPR angle was measured to quantify the target molecules (streptavidin) absorbed on the sensing substrate. As shown in Figure 5c, the system with biotinylated Ag@Au nanoplates showed 30 times enhancement of SPR signal after the surface was blocked by bovine serum albumin (BSA) than that of direct immobilization of streptavidin on the Au substrate. Compared with the biotinylated Au nanoparticles, which showed only 3 times enhancement than the control group, Ag@Au nanoplates were proved to be more efficient enhancers (Figure 5d). Importantly, the amplifying effect of the Ag@Au nanoplates was from the Ag core rather than the outside Au coating. It is worth noting that the high stability of Ag@Au nanoplates played a crucial role in the fabrication of the enhancers. Without the protection of Au, Ag nanoplates lost their plasmonic property immediately after biotinylation.

Recently, we have developed an improved method for the deposition of Au on Ag nanoplates. This method employed sulfite as the critical synthesis component.[50] Sulfite can reduce and coordinate to Au cations to form a very stable complex with a low reduction potential. The reduction potential of the Au (I)-sulfite complex (0.111 V vs. SHE) is much lower than that of Ag^+ (0.8 V vs. SHE). Thus, the Au (I) complex can be reduced by the addition of a reducing agent, rather than Ag. In this way, the galvanic replacement can be prevented

entirely. Also, since the interaction between the sulfite and Ag nanoparticles is weak, the use of the sulfite can prevent the Ag nanoparticles from ligand-assisted oxidative etching. Therefore, Au can be deposited on Ag nanoparticles continuously without involving any etching effect. As shown in Figure 6a, Ag@Au core-shell nanoplates with an edge length of ~55 nm and thickness of 9 nm were readily obtained in a high yield by using the sulfite as a coordinating agent for the growth of Au on Ag nanoplates. High-resolution TEM (HRTEM) images (Figure 6b) of the sample reveal that the Au layer was grown on the Ag nanoplates in a conformal epitaxial manner. The high-angle annular dark-field scanning transmission electron microscopy (HAADF-STEM) image and energy dispersive X-ray spectroscopy (EDS) elemental mapping (Figure 6c and d) show that the edges of the Ag@Au core-shell nanoplates were only composed of Au, because of the absence of the galvanic replacement. It is worth noting that the pH of the solution for the formation of Au (I)-sulfite should be maintained at 12. If the pH of the solution was adjusted to ~5, the Au(I)-sulfite complex could be destabilized, resulting in a controlled galvanic replacement that affords a holey nanostructure.[89] Figure 6e shows the SERS spectra recorded from aqueous solutions of crystal violet (CV, 10^{-5} M) enhanced by the Ag@Au and Ag nanoplates in the presence of Fe^{3+} and H_2O_2. When oxidative impurities presented in the analyte solution, the SERS signals from the Ag@Au nanoplates were well-maintained, whereas the SERS signals from Ag nanoplates decreased, indicating higher stability of the Ag@Au nanoplates in oxidative environment and reliability of such nanostructures in sensing. In addition, the detection limit of CV can be further reduced to ~10^{-8} M by depositing the Ag@Au nanoplates on silicon substrates (Figure 6f).
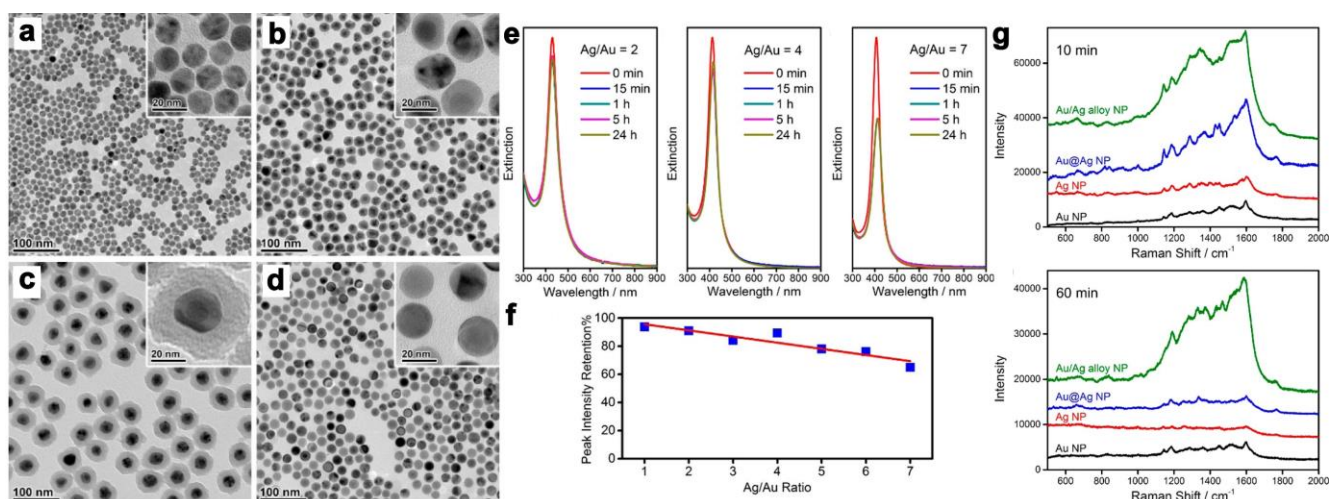
Fig. 7. TEM images of (a) Au nanoparticles, (b) Au@Ag core-shell nanoparticles, (c) Au@Ag@SiO$_2$ nanoparticles, and (d) Ag/Au alloy nanospheres obtained from a typical synthesis of Ag/Au alloy nanospheres (Ag/Au = 5). Chemical stability of the Ag/Au alloy nanospheres in an aqueous solution of H$_2$O$_2$ and NH$_3$·H$_2$O, as indicated by UV-vis spectral changes with time. (e) UV–vis spectra of nanospheres with Ag/Au = 2, 4, and 7, respectively, annealed at 1000 °C. (f) Change in the band intensity relative to the initial intensity after 24 h of etching as a function of the Ag/Au ratio. (g) SERS spectra of benzidine (0.5 μM) absorbed from an artificial industrial wastewater (2 wt % NaCl, 1 mM H$_2$O$_2$, pH 10) onto nanoparticle-loaded substrates by soaking the substrates in the wastewater for 10 and 60 min. Reprinted and modified from Ref. [55] with permission. Copyright 2014 American Chemical Society.

It is reported that plasmonic nanoparticles can assist photochemical transformations when illuminated with light of low intensity.[19] Nanocatalysts with enhanced performances could be achieved when combing plasmonic nanoparticles with a more active catalytic material. Aslam et al. reported the epitaxial growth of a few monolayers (~1 nm) of Pt on Ag nanocubes (~75 nm in length) for CO oxidation.[90] The Ag core could concentrate electromagnetic energy and the energy stored in the LSPR modes could be dissipated to form energetic charge carriers through the Pt shell, where the chemical reaction occurs. Besides Ag nanocubes, Ag nanoplates have also been used for the growth of Pt through a galvanic-replacement-free epitaxial growth process for the oxygen reduction reaction.[91] In addition, nanostructures integrating both plasmonic and catalytic properties can be used as bi-functional platforms for catalysis. Li et al. reported the fabrication of Ag@Pd-Ag nanocubes through a co-titration for the hydrogenation of p-nitrophenol by NaBH$_4$.[92] The core-shell nanostructures had Ag cores of 39 nm and Pt layer with a thickness of 1.1 nm. These nanoparticles could work as both SERS substrates and catalysts for monitoring the composition of the products at different stages of the catalytic reaction.

4. Stabilization of noble metal nanocrystals by forming alloys

Alloys of metal nanostructures have been widely investigated for sensing and catalysis to achieve high performances and stability.[93] Zhang group reported the synthesis of Au-Cu and Au-Ag nanoalloys for the CO oxidation reaction.[94, 95] The sizes of the Au-Cu and Au-Ag nanoalloys deposited on silica and alumina substrates remained unchanged after high-temperature treatment. Abdelsayed et al. investigated a wide variety of bimetallic alloy nanoparticles with controlled sizes and shapes toward the reaction of CO oxidation and

found out that the activity and thermal stability for the nanoalloys followed the order CuPd > CuRh > AuPd > AuRh > PtRh > PdRh > AuPt.[96] Also, magnetic nanoalloys have been reported as efficient and stable nanocatalysts.[97, 98]

Ag nanoparticles can be stabilized by forming alloys with Au. Conventional routes for the synthesis of Ag-Au alloys include laser ablation, phase-transfer, digestive ripening, co-reduction of both Au and Ag precursors, and galvanic replacement.[53, 99-102] All of the methods show drawbacks of causing compositional inhomogeneity in a single alloy nanoparticle. Compositional homogeneity is crucial to Au-Ag alloys to maintain morphological and optical stability. Moreover, the plasmonic property of the alloys may be affected by the interface of compositional domains. Domains with different composition of Au and Ag differ in dielectric properties, which may cause damping of surface plasmons and thus broadened bandwidths of the extinction spectrum, leading to limited applications of such particles.

We have developed a method to synthesize Ag-Au alloy nanospheres with the homogeneous composition of Ag and Au.[55] These alloy nanospheres combined the excellent plasmonic properties of Ag and the high stability of Au, showing strong LSPRs with narrow bandwidths and high resistivity to a corrosive environment. The synthesis started with the preparation of Au nanoparticles (~15 nm, Figure 7a) through a seeded growth method. Then, a thin layer of Ag was deposited on the surface of the Au nanoparticles to obtain a core-shell nanostructure (~22 nm, Figure 7b). The nanoparticles were further annealed at ~1000 ºC to achieve accelerated interfacial atomic diffusion of Ag and Au. Before annealing, the nanoparticles were coated with a layer of silica (~15 nm, Figure 7c) to prevent them from agglomeration in the high-temperature treatment. As shown in Figure 7d, pure Ag-Au alloys of 22 nm in sizes were achieved after etching the silica shells. It is worth noting that the high-temperature

annealing process had many influences on the Ag-Au alloys. First, the atomic mobility of Ag and Au was significantly enhanced at the high temperature, resulting in a release of crystallographic defects. Also, the high atomic mobility of the metals gave rise to the reshaping of the nanoparticles to form highly round ones in the silica shells. Moreover, the high diffusion rates of Ag and Au helped to generate fully alloyed nanoparticles. As a result, the obtained Ag-Au alloy nanoparticles were single crystalline, spherical and compositional homogenous. The ratio of Ag/Au could be adjusted by varying the amount of the Ag and Au precursors, respectively.

The stability of the Ag-Au alloy nanospheres was examined in a mixture of hydrogen peroxide and ammonia. The stability of the Ag-Au alloy nanospheres increased with the increase of the annealing temperature from 900 ºC to 1000 ºC. Upon etching, the plasmon band gradually decreased for the Ag-Au nanospheres alloyed at 900 ºC. In contrast, the Ag-Au nanospheres alloyed at 930 ºC remained 82 % of the plasmon band intensity after etching for 24 h. Also, the stability of the Ag-Au alloy nanospheres depended on the Ag/Au ratio. As shown in Figure 7e and f, the UV-vis extinction of the Ag/Au alloy nanospheres with Ag/Au = 7 retained 65% of their original intensity after 24 h of etching in an aqueous solution of H_2O_2 and $NH_3 \cdot H_2O$, while the alloy nanospheres with lower Ag/Au ratios retained much higher percentage of their initial UV-vis extinctions. The Ag-Au alloy nanospheres were used for detection of benzidine in artificial wastewater mimicked by NaCl, H_2O_2, and NaOH, which are commonly present in industrial wastewater. As shown in Figure 7g, compared with Au, Ag and Au@Ag nanoparticles, the Au-Ag alloy nanospheres showed much stable and strong SERS responses, which were independent of the soaking time, indicating the promising application of such alloy nanoparticles in corrosive conditions.

This approach has recently been extended to the fabrication of fully alloyed anisotropic Ag/Au nanorods.[103] As expected, the alloy nanorods showed superior chemical stability against etching in H_2O_2 and $NH_3 \cdot H_2O$. Moreover, the wavelength and intensity of both transverse and longitudinal modes of the alloy NRs could be tailored by simply controlling the Ag/Au ratio and their aspect ratio.

5. Conclusion and perspectives

In this article, we summarize our recent progress on the stabilization of noble metal nanocrystals through various approaches, including using inorganic and non-metal solids as supports and physical barriers, coating metal nanocrystals with another metal species with higher stability, and forming alloys. Inorganic and non-metal solids have been widely employed for the stabilization of metal nanocrystals. Creation of a physical barrier by inorganic coating significantly enhances the stability of metal nanocrystals during the reactions. To improve the permeability of the shells, we have made efforts in controlling the shell porosity by a surface-protected etching process. With control of the shell porosity, better diffusion of reactants to the surface of the catalysts can be achieved. Also, we discussed the metal coating method for stabilizing Ag nanostructures against chemical etching, while maintaining the structural and plasmonic properties of Ag nanostructures as well. To suppress the galvanic replacement of Ag nanostructures in the coating of Au, some ligands, such as I^- and SO_3^{2-}, have been used to form stable complexes with the Au salt, leading to a significantly reduced reduction

potential of the Au cations. Finally, we discussed the preparation and properties of Ag-Au alloys by calcination of Au@Ag core/shell nanoparticles with the protection of a silica layer. The alloys show excellent plasmonic property and significantly improved stability against chemical etching.

Although the above-discussed approaches have shown great promises in enhancing the thermal and chemical stability of the noble metal nanocrystals, there are still many remaining challenges that limit the practical applications of the noble metal nanocrystals. One has to design appropriate strategies to address different challenges for sensing and catalysis where the specific conditions and requirements are different. The following are our thoughts on the challenges and future research directions in the relevant fields.

1) In the coating method by using inorganic and non-metal solids, if the control over the pore size and distribution in the inorganic shells could be further improved, one may be able to afford high selectivity in the permeation of reactants based on their sizes. The inorganic shells discussed here are mostly microporous, which are not suitable for catalytic reactions involving large molecules. The surface protected etching method can produce much larger pores, which however have a very wide size distribution, making them impropriate for size-selective catalytic reactions. The surfactant-templated synthesis strategy, widely developed previously for creating highly ordered mesoscale porosity in bulk inorganic solids, may be adapted to create protective shells containing narrowly distributed pores with sizes relevant to many important catalytic reactions. However, the surfactant-templated strategy is known to be inflexible in tuning the pore sizes continuously over a reasonable range. As a result, fine-tuning the size of the pores to match that of the reactants to maximize the size-selectivity could still be challenging. To this end, it may be worth pursuing to add an etching step to the surfactant-templated strategy so that the mesopores can be widened within a certain range. While the etching method may have difficulty in uniformly increasing the pore size in the bulk samples due to the inhomogeneity in the diffusion of the etchants over a long distance in the pores, this may be feasible in mesoporous shells thanks to the short diffusion paths.

2) Additional efforts are needed to develop inorganic and non-metal solids other than the conventionally used ones including SiO_2, TiO_2, and carbon. Many inorganic support materials have shown the ability in enhancing the performance of the catalysts through effects such as spillover and strong metal-support interactions.[104, 105] It is therefore highly desirable to explore effective methods for coating metal nanocrystals with other inorganic solids such as Al_2O_3, CeO_2, ZrO_2, Fe_2O_3, etc. as these materials as nanoshells may not only stabilize the metal nanoparticles but also provide opportunities for improving the catalytic selectivity and activity.

3) For the stability of catalysts, not only their sizes and agglomeration states but also their morphologies are concerned. The significant advances in the nanoscale synthesis in the past decades have made it possible to precisely control the morphology of the nanostructured catalysts so that they are enriched with active facets toward particular catalytic reactions. These facets are often the high-energy ones, and they can quickly disappear during the catalytic reactions in accompany with the change of the overall morphologies. The employment of protective shells can effectively prevent the sintering and agglomeration of the nanocatalysts, but not their morphology

changes. To address this issue, one may need to look into shell materials that can exhibit strong interactions with the catalysts and accordingly minimize the disturbance to the active facets during the catalytic reactions.

4) Enhancing the utilization efficiency of the catalyst is especially important to large-scale reactions that involve noble metal catalysts. In addition to making them smaller, another strategy is to deposit noble metals on the surface of non-noble metal nanocrystals and bring more catalytically active atoms to the surface. For example, one can deposit a thin layer of Pt onto Ni nanoparticles to greatly reduce the overall cost of the catalysts. To be useful to practical catalytic applications, the nanoparticles need to be small in size. In addition, it is desirable to use cheaper and more earth-abundant transition metals such as Cu, Fe, Co, and Ni as the cores. Since the cores are more reactive than the Ag nanocrystals demonstrated in our previous cases, the deposition of noble metals on their surfaces requires more careful management of the reaction kinetics. On the other hand, a carefully controlled deposition process may take full advantage of the lattice mismatch between the two metals and create highly active facets that are difficult to obtain with pure noble metals, offering many opportunities in enhancing the activity and selectivity of the catalytic reactions.

5) In the alloying method, it would be an interesting subject to study how the addition of two or more metals affects the chemical and morphological stability and optical and catalytic properties of the resulting alloy nanostructures. For catalytic applications, it is also critical to understand the distribution and arrangement of different metal species on the surface of the alloy nanostructures, which is expected to contribute significantly to the activity and selectivity of the catalysts. The synergistic interactions of the metals in these alloy nanostructures are critical to the improvement of the catalytic performance and therefore worth being fully explored in a broad range of reactions. For sensing applications, understanding the atomic distribution and surface structure of the alloy nanoparticles is also expected to help design surfaces with higher affinity to the analytes. It is also interesting to study the synthesis of metal alloy nanostructures with well-controlled morphologies to enhance the electro-optical properties such as optical absorption, scattering, and polarization. By fine-tuning the surface structure and controlling the electro-optical properties, we may be able to design sensors with significantly improved sensing performance.

Conflicts of interest

There are no conflicts to declare.

Acknowledgements

Notes and references

1. D. I. Enache, J. K. Edwards, P. Landon, B. Solsona-Espriu, A. F. Carley, A. A. Herzing, M. Watanabe, C. J. Kiely, D. W. Knight and G. J. Hutchings, *Science*, 2006, **311**, 362-365.
2. W. Oppolzer, *Angew. Chem., Int. Ed.*, 1989, **28**, 38-52.
3. Y. Xing, *J. Phys. Chem. B*, 2004, **108**, 19255-19259.
4. S. U. M. Khan, M. Al-Shahry and W. B. Ingler, *Science*, 2002, **297**, 2243-2245.
5. K. Maeda, K. Teramura, D. Lu, T. Takata, N. Saito, Y. Inoue and K. Domen, *Nature*, 2006, **440**, 295-295.
6. M. Ni, M. K. H. Leung, D. Y. C. Leung and K. Sumathy, *Renew. Sust. Energ. Rev.*, 2007, **11**, 401-425.
7. G. J. Hutchings and M. Haruta, *Appl. Catal., A*, 2005, **291**, 2-5.
8. M. Haruta, N. Yamada, T. Kobayashi and S. Iijima, *J. Catal.*, 1989, **115**, 301-309.
9. Y. Xiong, B. J. Wiley and Y. Xia, *Angew. Chem., Int. Ed.*, 2007, **46**, 7157-7159.
10. N. Pernicone, *CATTECH*, 2003, **7**, 196-204.
11. I. Lee, F. Delbecq, R. Morales, M. A. Albiter and F. Zaera, *Nat. Mater.*, 2009, **8**, 132-138.
12. J. W. Hong, Y. Kim, Y. Kwon and S. W. Han, *Chem. Asian J.*, 2016, **11**, 2224-2239.
13. L. Liu and A. Corma, *Chem. Rev.*, 2018, **118**, 4981-5079.
14. S. Mostafa, F. Behafarid, J. R. Croy, L. K. Ono, L. Li, J. C. Yang, A. I. Frenkel and B. R. Cuenya, *J. Am. Chem. Soc.*, 2010, **132**, 15714-15719.
15. K. M. Mayer and J. H. Hafner, *Chem. Rev.*, 2011, **111**, 3828-3857.
16. S. Yu, A. J. Wilson, J. Heo and P. K. Jain, *Nano Lett.*, 2018, **18**, 2189-2194.
17. F. Wang, C. Li, H. Chen, R. Jiang, L.-D. Sun, Q. Li, J. Wang, J. C. Yu and C.-H. Yan, *J. Am. Chem. Soc.*, 2013, **135**, 5588-5601.
18. B. Y. Zheng, H. Zhao, A. Manjavacas, M. McClain, P. Nordlander and N. J. Halas, *Nat. Commun.*, 2015, **6**, 7797.
19. P. Christopher, H. Xin and S. Linic, *Nat. Chem.*, 2011, **3**, 467.
20. P. Christopher, H. Xin, A. Marimuthu and S. Linic, *Nat. Mater.*, 2012, **11**, 1044.
21. S. Zhou, J. Li, K. D. Gilroy, J. Tao, C. Zhu, X. Yang, X. Sun and Y. Xia, *ACS Nano*, 2016, **10**, 9861-9870.
22. A. Ruditskiy and Y. Xia, *J. Am. Chem. Soc.*, 2016, **138**, 3161-3167.
23. J. J. Mock, D. R. Smith and S. Schultz, *Nano Lett.*, 2003, **3**, 485-491.
24. J. Lu, B. Fu, M. C. Kung, G. Xiao, J. W. Elam, H. H. Kung and P. C. Stair, *Science*, 2012, **335**, 1205-1208.
25. I. Lee, Q. Zhang, J. Ge, Y. Yin and F. Zaera, *Nano Res.*, 2011, **4**, 115-123.
26. I. Pastoriza-Santos and L. M. Liz-Marzán, *Langmuir*, 1999, **15**, 948-951.
27. L. M. Liz-Marzán and I. Lado-Touriño, *Langmuir*, 1996, **12**, 3585-3589.
28. L. Kvítek, A. Panáček, J. Soukupová, M. Kolář, R. Večeřová, R. Prucek, M. Holecová and R. Zbořil, *J. Phys. Chem. C*, 2008, **112**, 5825-5834.
29. I. Pastoriza-Santos and L. M. Liz-Marzán, *Langmuir*, 2002, **18**, 2888-2894.
30. M. H. Ullah, W. S. Chung, I. Kim and C. S. Ha, *Small*, 2006, **2**, 870-873.
31. Y. Mizukoshi, T. Fujimoto, Y. Nagata, R. Oshima and Y. Maeda, *J. Phys. Chem. B*, 2000, **104**, 6028-6032.
32. R. Dun, X. Wang, M. Tan, Z. Huang, X. Huang, W. Ding and X. Lu, *ACS Catalysis*, 2013, **3**, 3063-3066.
33. C. Huang, C. Chen, X. Ye, W. Ye, J. Hu, C. Xu and X. Qiu, *J. Mater. Chem. A*, 2013, **1**, 12192-12197.
34. I. Washio, Y. Xiong, Y. Yin and Y. Xia, *Adv. Mater.*, 2006, **18**, 1745-1749.

35. W. C. Elias, R. Eising, T. R. Silva, B. L. Albuquerque, E. Martendal, L. Meier and J. B. Domingos, *J. Phys. Chem. C*, 2014, **118**, 12962-12971.

36. Z.-J. Jiang, C.-Y. Liu and L.-W. Sun, *J. Phys. Chem. B*, 2005, **109**, 1730-1735.

37. Q. Fan, K. Liu, Z. Liu, H. Liu, L. Zhang, P. Zhong and C. Gao, *Part. Part. Syst. Char.*, 2017, **34**, 1700075.

38. N. V. Long, Y. Yang, C. Minh Thi, N. V. Minh, Y. Cao and M. Nogami, *Nano Energy*, 2013, **2**, 636-676.

39. Z. Li, M. Li, Z. Bian, Y. Kathiraser and S. Kawi, *Appl. Catal., B*, 2016, **188**, 324-341.

40. H. Hu, J. H. Xin and H. Hu, *J. Mater. Chem. A*, 2014, **2**, 11319-11333.

41. I. Fampiou and A. Ramasubramaniam, *J. Phys. Chem. C*, 2012, **116**, 6543-6555.

42. M. Liu, R. Zhang and W. Chen, *Chem. Rev.*, 2014, **114**, 5117-5160.

43. J. Zhou, Y. Zhao, J. Zhang, Y. Wang, O. Y. Gutierrez, S. Wang, Z. Li, P. Jin, S. Wang, X. Ma and J. A. Lercher, *Chem. Commun.*, 2018, **54**, 8818-8821.

44. Q. Wu, B. Yan, J. Cen, J. Timoshenko, D. N. Zakharov, X. Chen, H. L. Xin, S. Yao, J. B. Parise, A. I. Frenkel, E. A. Stach, J. G. Chen and A. Orlov, *Chem. Mater.*, 2018, **30**, 1585-1592.

45. H. Tang, J. Wei, F. Liu, B. Qiao, X. Pan, L. Li, J. Liu, J. Wang and T. Zhang, *J. Am. Chem. Soc.*, 2016, **138**, 56-59.

46. H. Woo, J. C. Park, S. Park and K. H. Park, *Nanoscale*, 2015, **7**, 8356-8360.

47. M. Ye, Q. Zhang, Y. Hu, J. Ge, Z. Lu, L. He, Z. Chen and Y. Yin, *Chem. Eur. J.*, 2010, **16**, 6243-6250.

48. C. Hanske, M. N. Sanz - Ortiz and L. M. Liz - Marzán, *Adv. Mater.*, 2018, **0**, 1707003.

49. M. M. Shahjamali, M. Bosman, S. Cao, X. Huang, S. Saadat, E. Martinsson, D. Aili, Y. Y. Tay, B. Liedberg, S. C. J. Loo, H. Zhang, F. Boey and C. Xue, *Adv. Funct. Mater.*, 2012, **22**, 849-854.

50. H. Liu, T. Liu, L. Zhang, L. Han, C. Gao and Y. Yin, *Adv. Funct. Mater.*, 2015, **25**, 5435-5443.

51. Z. Li, X. Miao, K. Xing, X. Peng, A. Zhu and L. Ling, *Biosens. Bioelectron.*, 2016, **80**, 339-343.

52. X. Miao, S. Zou, H. Zhang and L. Ling, *Sens. Actuators, B*, 2014, **191**, 396-400.

53. M. J. Hostetler, C.-J. Zhong, B. K. H. Yen, J. Anderegg, S. M. Gross, N. D. Evans, M. Porter and R. W. Murray, *J. Am. Chem. Soc.*, 1998, **120**, 9396-9397.

54. S. E. Skrabalak, J. Chen, Y. Sun, X. Lu, L. Au, C. M. Cobley and Y. Xia, *Acc. Chem. Res.*, 2008, **41**, 1587-1595.

55. C. Gao, Y. Hu, M. Wang, M. Chi and Y. Yin, *J. Am. Chem. Soc.*, 2014, **136**, 7474-7479.

56. Q. Zhang and Y. Yin, *Pure Appl. Chem.*, 2014, **86**, 53-69.

57. Y.-S. Chi, H.-P. Lin and C.-Y. Mou, *Appl. Catal., A*, 2005, **284**, 199-206.

58. X. Liu, X. Cui, Y. Liu and Y. Yin, *Nanoscale*, 2015, **7**, 18320-18326.

59. T. Ung, L. M. Liz-Marzán and P. Mulvaney, *Langmuir*, 1998, **14**, 3740-3748.

60. K. Aslan, M. Wu, J. R. Lakowicz and C. D. Geddes, *J. Am. Chem. Soc.*, 2007, **129**, 1524-1525.

61. C. Graf, D. L. J. Vossen, A. Imhof and A. van Blaaderen, *Langmuir*, 2003, **19**, 6693-6700.

62. J. Pak and H. Yoo, *J. Mater. Chem. A*, 2013, **1**, 5408-5413.

63. J. Wang, W. B. White and J. H. Adair, *Mater. Sci. Ene. B-Adv.*, 2010, **166**, 235-238.

64. D.-S. Bae, K.-S. Han and J. H. Adair, *J. Am. Ceram. Soc.*, 2002, **85**, 1321-1323.

65. M. Kim, E. Heo, A. Kim, J. Park, H. Song and K. Park, *Catal. Lett.*, 2012, **142**, 588-593.

66. T. Tago, Y. Shibata, T. Hatsuta, K. Miyajima, M. Kishida, S. Tashiro and K. Wakabayashi, *J. Mater. Sci.*, 2002, **37**, 977-982.

67. K. A. Dahlberg and J. W. Schwank, *Chem. Mater.*, 2012, **24**, 2635-2644.

68. Y. Han, J. Jiang, S. S. Lee and J. Y. Ying, *Langmuir*, 2008, **24**, 5842-5848.

69. T. Zhang, H. Zhao, S. He, K. Liu, H. Liu, Y. Yin and C. Gao, *ACS Nano*, 2014, **8**, 7297-7304.

70. S. H. Joo, J. Y. Park, C.-K. Tsung, Y. Yamada, P. Yang and G. A. Somorjai, *Nat. Mater.*, 2008, **8**, 126.

71. Q. Zhang, T. Zhang, J. Ge and Y. Yin, *Nano Lett.*, 2008, **8**, 2867-2871.

72. J. Goebl and Y. Yin, *Chemcatchem*, 2013, **5**, 1287-1288.

73. M. Xiao, C. Zhao, H. Chen, B. Yang and J. Wang, *Adv. Funct. Mater.*, 2012, **22**, 4526-4532.

74. H. Zhao, D. Wang, C. Gao, H. Liu, L. Han and Y. Yin, *J. Mater. Chem. A*, 2016, **4**, 1366-1372.

75. Q. Zhang, D. Q. Lima, I. Lee, F. Zaera, M. Chi and Y. Yin, *Angew. Chem.*, 2011, **123**, 7226-7230.

76. I. Lee, J. B. Joo, Y. Yin and F. Zaera, *Angew. Chem., Int. Ed.*, 2011, **50**, 10208-10211.

77. W. Ye, R. Long, H. Huang and Y. Xiong, *J. Mater. Chem. C*, 2017, **5**, 1008-1021.

78. Y. C. Cao, R. Jin and C. A. Mirkin, *Science*, 2002, **297**, 1536-1540.

79. K.-S. Lee and M. A. El-Sayed, *J. Phys. Chem. B*, 2006, **110**, 19220-19225.

80. C. Ying, W. Chungang, M. Zhanfang and S. Zhongmin, *Nanotechnol.*, 2007, **18**, 325602.

81. B. Tang, J. An, X. Zheng, S. Xu, D. Li, J. Zhou, B. Zhao and W. Xu, *J. Phys. Chem. C*, 2008, **112**, 18361-18367.

82. Q. Zhang, J. Ge, T. Pham, J. Goebl, Y. Hu, Z. Lu and Y. Yin, *Angew. Chem.*, 2009, **121**, 3568-3571.

83. C. Xue, X. Chen, S. J. Hurst and C. A. Mirkin, *Adv. Mater.*, 2007, **19**, 4071-4074.

84. M.-K. Nguyen, W.-N. Su, C.-H. Chen, J. Rick and B.-J. Hwang, *Spectrochim. Acta A Mol. Biomol. Spectrosc.*, 2017, **175**, 239-245.

85. L. Au, X. Lu and Y. Xia, *Adv. Mater.*, 2008, **20**, 2517-2522.

86. Y. Yang, J. Liu, Z.-W. Fu and D. Qin, *J. Am. Chem. Soc.*, 2014, **136**, 8153-8156.

87. X. Sun, Y. Yang, Z. Zhang and D. Qin, *Chem. Mater.*, 2017, **29**, 4014-4021.

88. C. Gao, Z. Lu, Y. Liu, Q. Zhang, M. Chi, Q. Cheng and Y. Yin, *Angew. Chem., Int. Ed.*, 2012, **51**, 5629-5633.

89. X. Wei, Q. Fan, H. Liu, Y. Bai, L. Zhang, H. Zheng, Y. Yin and C. Gao, *Nanoscale*, 2016, **8**, 15689-15695.

90. U. Aslam, S. Chavez and S. Linic, *Nat. Nanotechnol.*, 2017, **12**, 1000-1006.

91. H. Liu, P. Zhong, K. Liu, L. Han, H. Zheng, Y. Yin and C. Gao, *Chemical Science*, 2018, **9**, 398-404.

92. J. Li, J. Liu, Y. Yang and D. Qin, *J. Am. Chem. Soc.*, 2015, **137**, 7039-7042.

93. A. K. Singh and Q. Xu, *ChemCatChem*, 2013, **5**, 652-676.

94. X. Liu, A. Wang, X. Wang, C.-Y. Mou and T. Zhang, *Chem. Commun.*, 2008, DOI: 10.1039/B804362K, 3187-3189.

95. X. Liu, A. Wang, X. Yang, T. Zhang, C.-Y. Mou, D.-S. Su and J. Li, *Chem. Mater.*, 2009, **21**, 410-418.

96. V. Abdelsayed, A. Aljarash, M. S. El-Shall, Z. A. Al Othman and A. H. Alghamdi, *Chem. Mater.*, 2009, **21**, 2825-2834.

97. J.-M. Yan, X.-B. Zhang, S. Han, H. Shioyama and Q. Xu, *J. Power Sources*, 2009, **194**, 478-481.

98. C. F. Yao, L. Zhuang, Y. L. Cao, X. P. Ai and H. X. Yang, *Int. J. Hydrogen Energy*, 2008, **33**, 2462-2467.

99. I. Lee, S. W. Han and K. Kim, *Chem. Commun.*, 2001, DOI: 10.1039/B105437F, 1782-1783.

100. S. Link, Z. L. Wang and M. A. El-Sayed, *J. Phys. Chem. B*, 1999, **103**, 3529-3533.

101. X. Xia, Y. Wang, A. Ruditskiy and Y. Xia, *Adv. Mater.*, 2013, **25**, 6313-6333.

102. M. P. Mallin and C. J. Murphy, *Nano Lett.*, 2002, **2**, 1235-1237.

103. Y. Bai, C. Gao and Y. Yin, *Nanoscale*, 2017, **9**, 14875-14880.

104. W. C. Conner and J. L. Falconer, *Chem. Rev.*, 1995, **95**, 759-788.

105. S. J. Tauster, *Acc. Chem. Res.*, 1987, **20**, 389-394.

TOC Graphics:

Stabilization of noble metal nanostructures